Supporting Information for

General synthesis for supported single-atom catalysts using hydroxyl nests in zeolites

Qiang Liu,[a] Jingnan Wang, [b] Kaiheng Zhao,[c] Yongan Yang[d] and Xi Wang [*e,f]

[a] School of Chemical Engineering and Technology, Tianjin University, Molecular Plus and Collaborative Innovation Center of Chemical Science and Engineering, Tianjin, China

[b] Molecular Engineering Plus, College of Chemistry, Fuzhou University, Fuzhou 350108, China

[c] Key Laboratory of Photochemistry Institute of Chemistry, Chinese Academy of Sciences, Beijing 100190, China

[d] Institute of Molecular Plus, Department of Chemistry, Tianjin University, Tianjin 300072, China

[e] Key Laboratory of Luminescence and Optical Information, Ministry of Education, School of Physical Science and Engineering, Beijing Jiaotong University, Beijing 100044, China

[f] Tangshan Research Institute of Beijing Jiaotong University, Tangshan 063000, China

KEYWORDS: Single-atom catalysts, High-temperature catalysis, Hydroxyl-nests, Propane dehydrogenation, General synthesis.

*** Corresponding author**

Email: xiwang@bjtu.edu.cn

Equations:

Corrected peak area:

$$A_i = nA_jF_j$$

A_i was the relative quantity of the hydrocarbon products, n was the carbon number of hydrocarbons, A_j was the peak area given by the FID results, and F_j was the relative correction factor.

Propane conversion was calculated as follows:

$$\text{Conversion} = \frac{\Sigma A_i}{\Sigma A_i + A_{C_3H_8}}$$

The selectivity of hydrocarbon products is calculated as follows:

$$\text{Selectivity}_i = \frac{A_i}{\Sigma A_i}$$

The yield of hydrocarbon products is calculated as follows:

$$\text{Yield} = \frac{A_i}{\Sigma A_i + A_{C_3H_8}}$$

Carbon balance (> 95%) is calculated as follows:

$$\text{Carbon balance} = \frac{\Sigma A_i}{A_{C_3H_8}}$$

The deactivation rate is calculated as follows:

$$k_d(h^{-1}) = \frac{\ln\left(\frac{1-Xend}{Xend}\right) - \ln\left(\frac{1-Xstart}{Xstart}\right)}{t}$$

where Xstart and Xend represent the conversion at the start and the end of an experiment, and t is the duration of the experiment in hours, higher k_d values being indicative of rapid deactivation, that is, low stability.

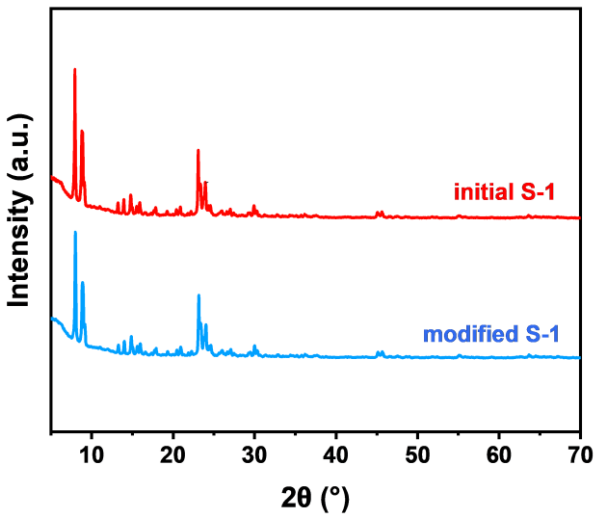

Figure S1. The XRD spectra of S-1 zeolite.

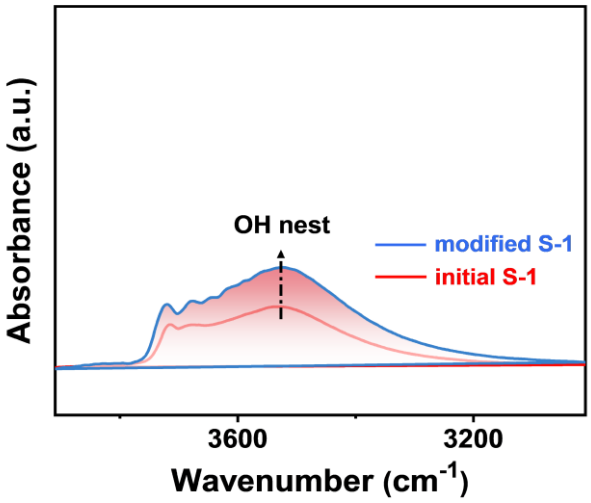

Figure S2 The IR spectra of S-1 zeolite.

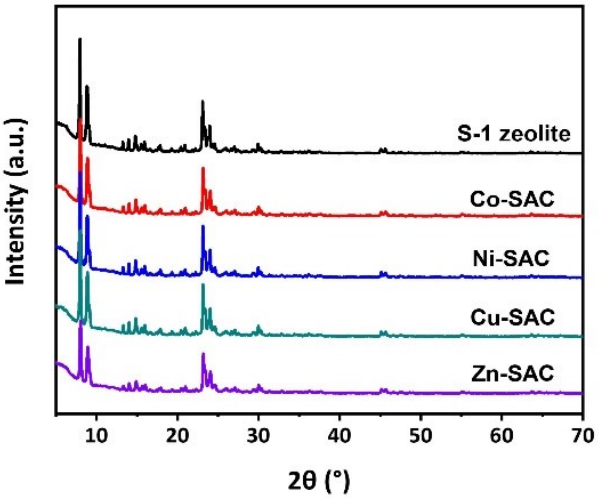

Figure S3 The XRD patterns of M-SACs.

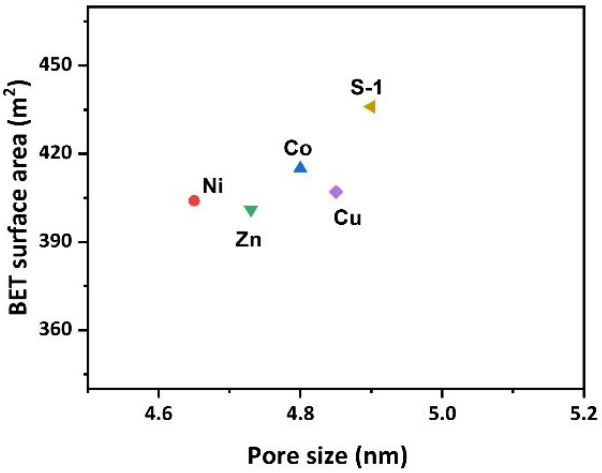

Figure S4 The physical properties data of different catalysts.

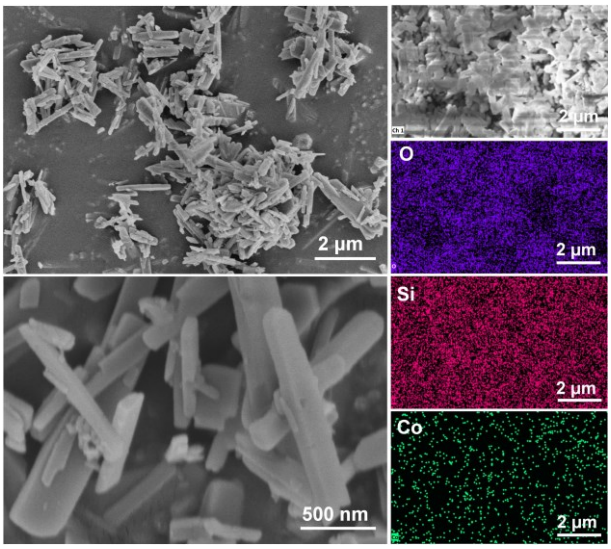

Figure S5 The SEM images and the corresponding EDS mapping images of the Co-SAC catalyst.

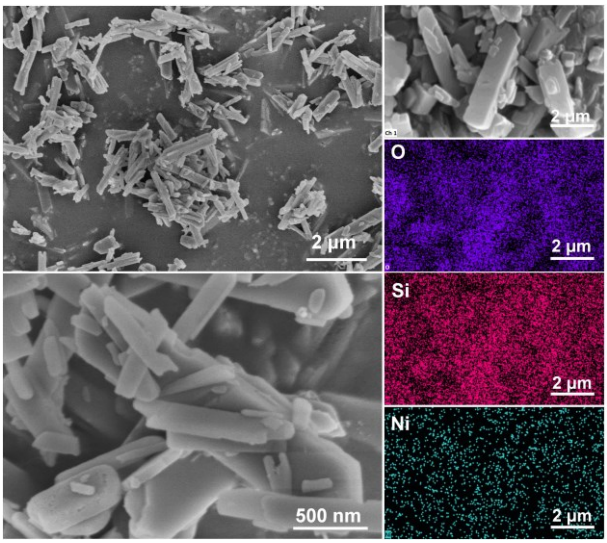

Figure S6 The SEM images and the corresponding EDS mapping images of the Ni-SAC.

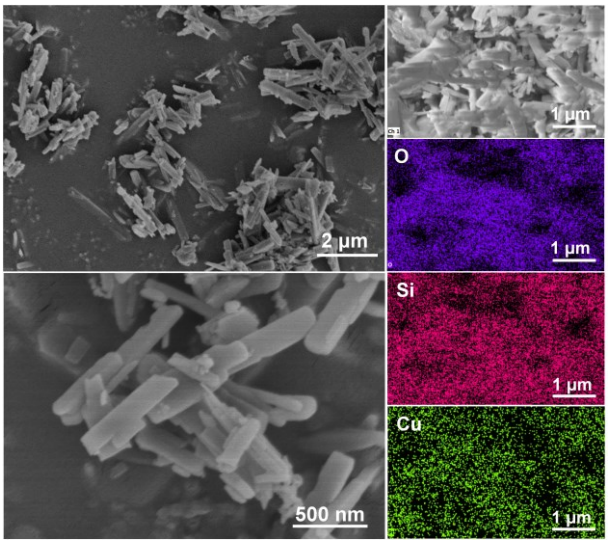

Figure S7 The SEM images and the corresponding EDS mapping images of the Cu-SAC.

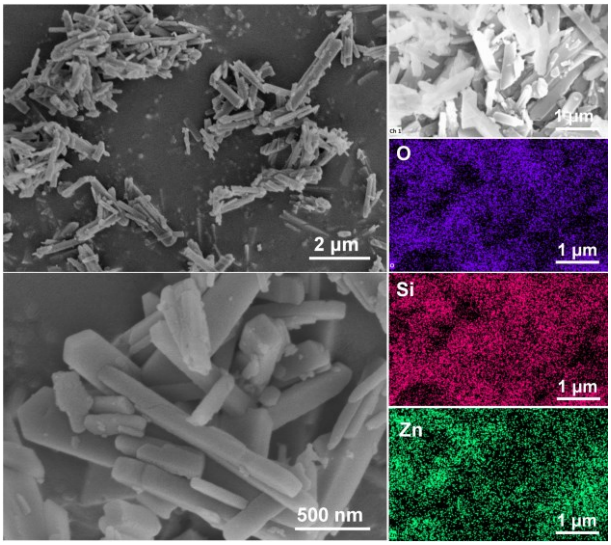

Figure S8 The SEM images and the corresponding EDS mapping images of the Zn-SAC.

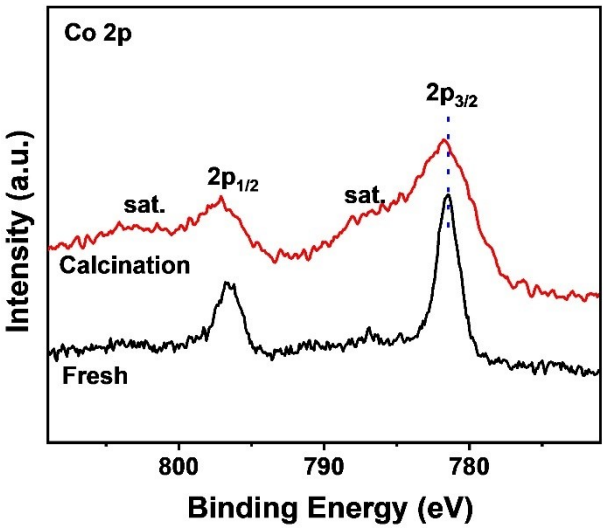

Figure S9 The XPS spectra of the Co-SAC catalysts: fresh catalysts and after calcination.

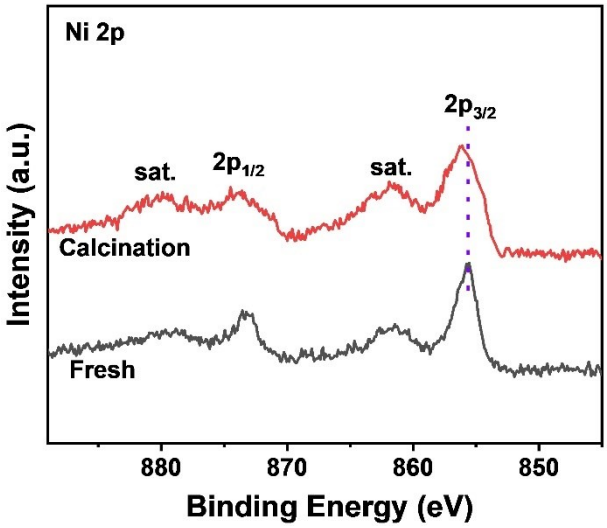

Figure S10 XPS spectra of the Ni-SAC catalysts: fresh catalysts and after calcination.

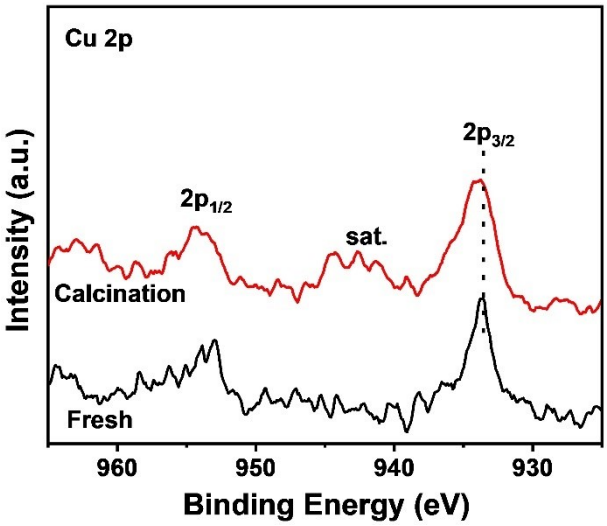

Figure S11 The XPS spectra of the Cu-SAC catalysts: fresh catalysts and after calcination.

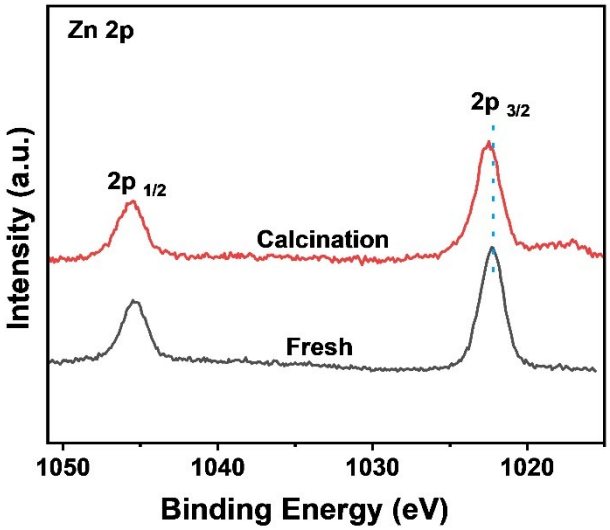

Figure S12 The XPS spectra of the Zn-SAC catalysts: fresh catalysts and after calcination.

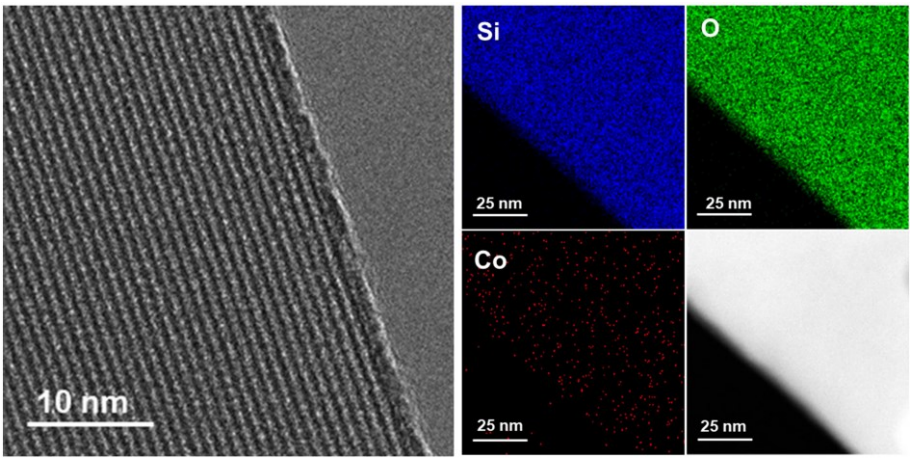

Figure S13 TEM image and the corresponding EDS mapping images of Co-SAC.

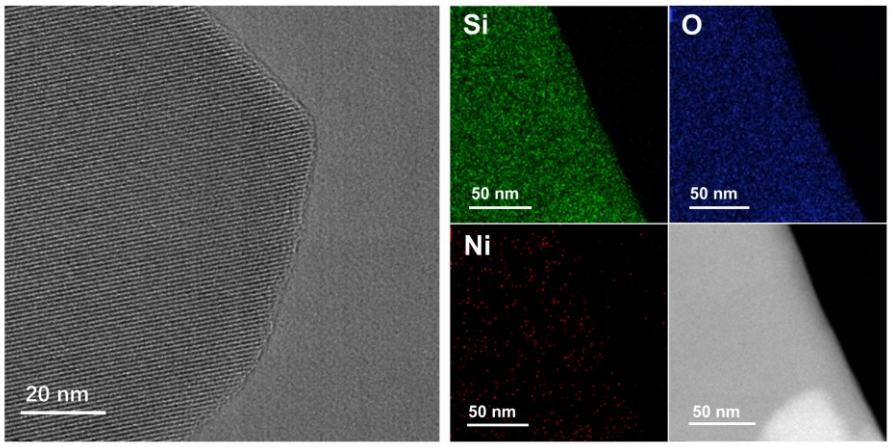

Figure S14 TEM image and the corresponding EDS mapping images of Ni-SAC.

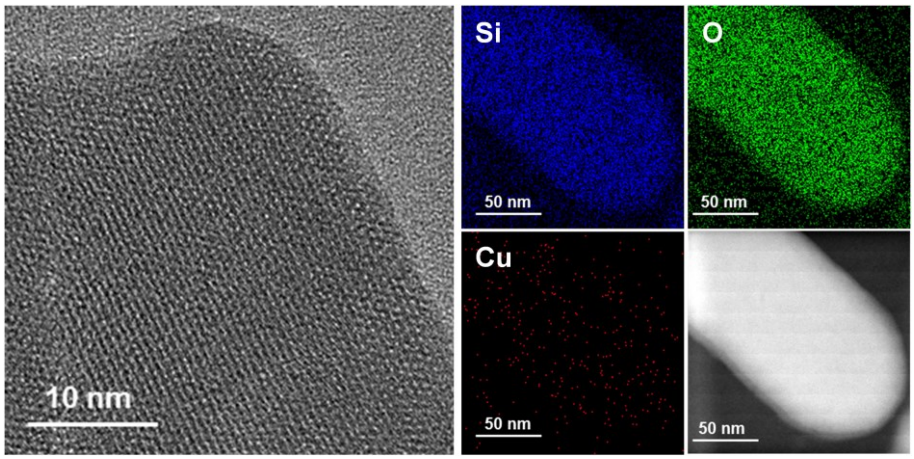

Figure S15 TEM image and the corresponding EDS mapping images of Cu-SAC.

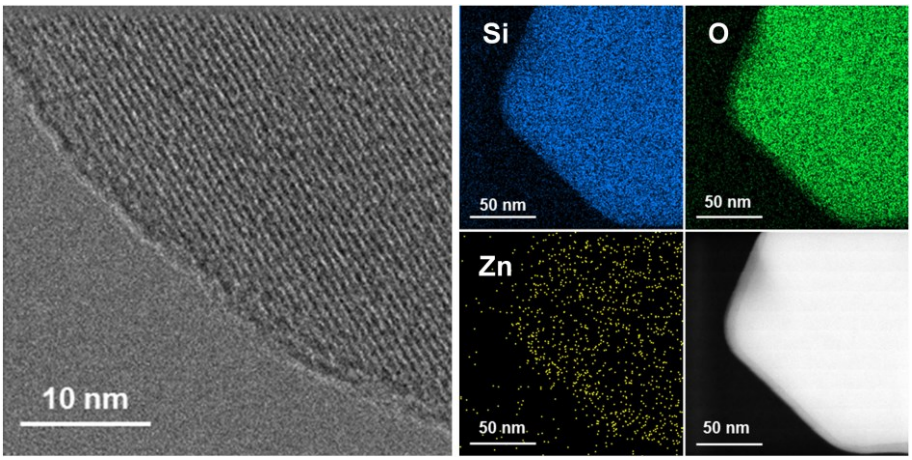

Figure S16 TEM image and the corresponding EDS mapping images of Zn-SAC.

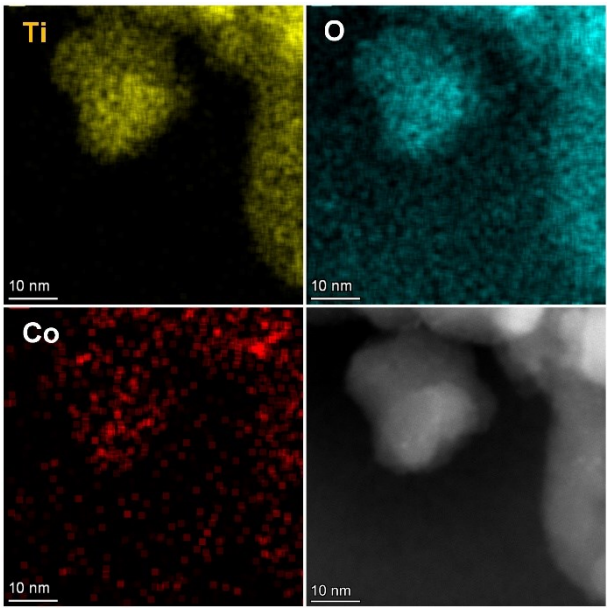

Figure S17 HADDF-STEM image and the corresponding EDS mapping images of the Co/TiO_2 catalyst.

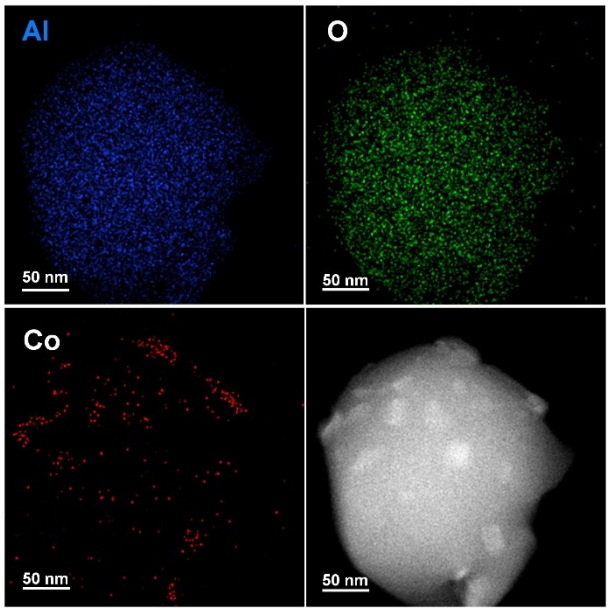

Figure S18 HADDF-STEM image and the corresponding EDS mapping images of the Co/SiO_2 catalyst.

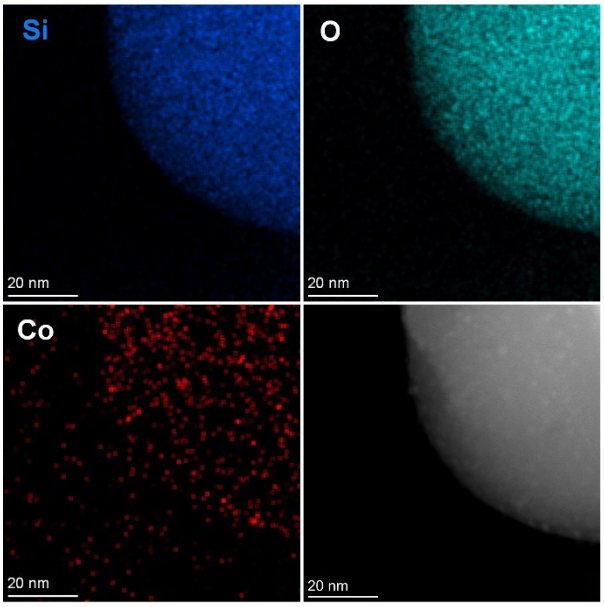

Figure S19 HADDF-STEM image and the corresponding EDS mapping images of the Co/Al_2O_3 catalyst.

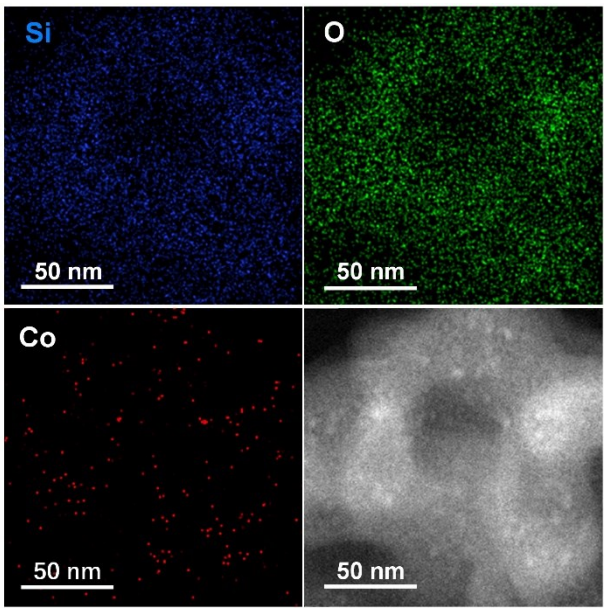

Figure S20 HADDF-STEM image and the corresponding EDS mapping images of the Co/MCM-41. catalyst.

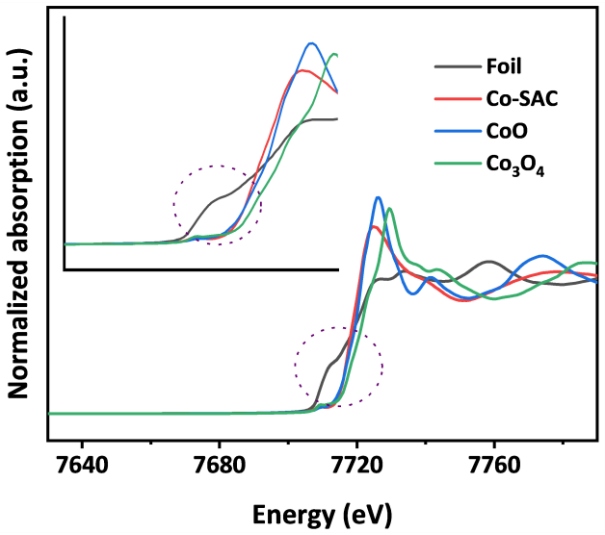

Figure S21 The K-edge near-edge XANES spectra of Co-SAC.

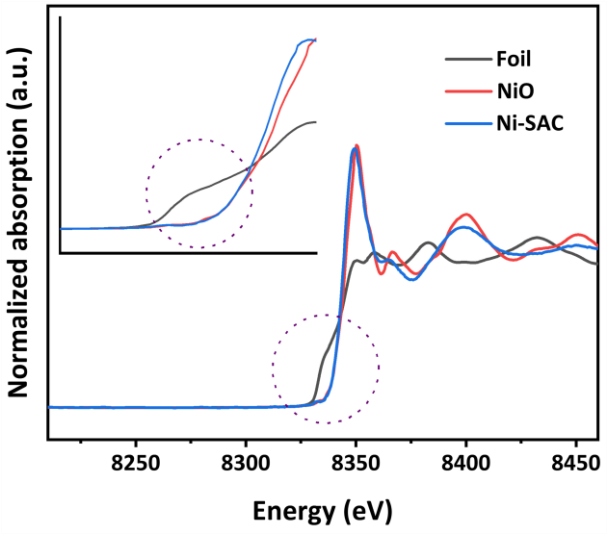

Figure S22 The K-edge near-edge XANES spectra of Ni-SAC.

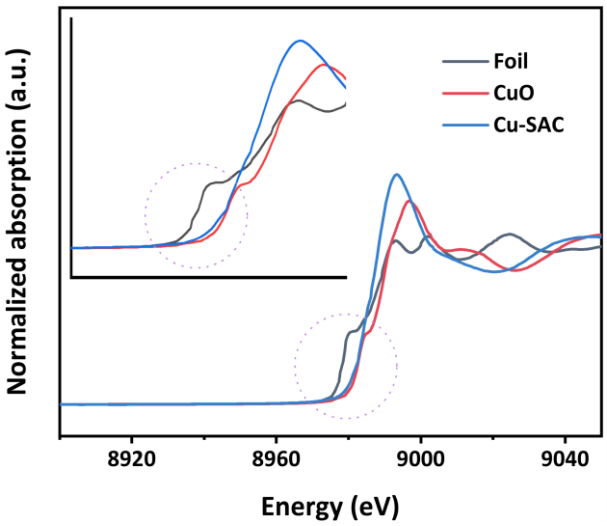

Figure S23 The K-edge near-edge XANES spectra of Cu-SAC.

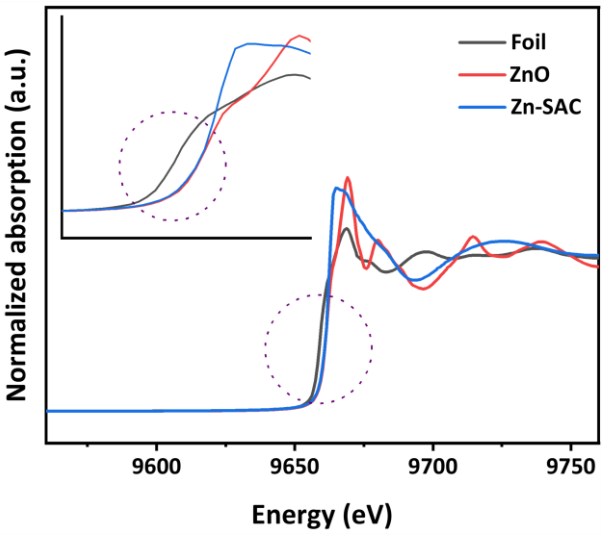

Figure S24 The K-edge near-edge XANES spectra of Zn-SAC.

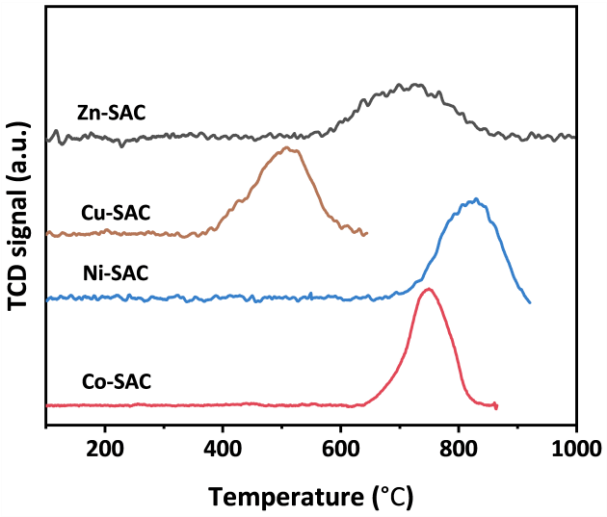

Figure S25 The H_2-TPR curve of M-SACs.

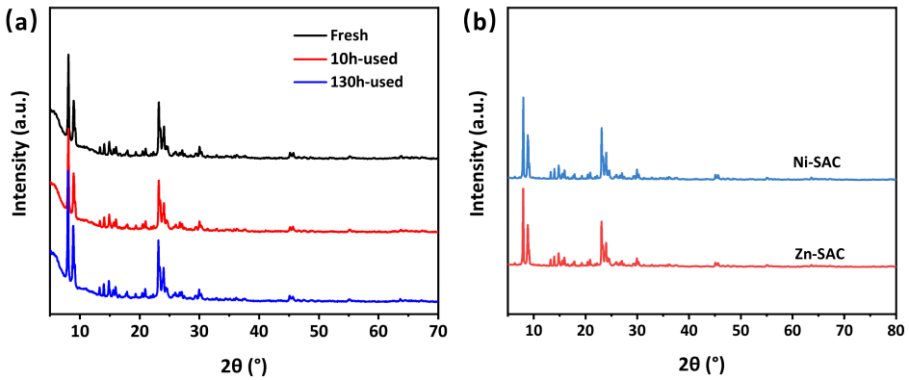

Figure S26 The XRD patterns of Co-SAC catalysts after reaction (a) and M-SAC catalysts after 10 h reaction (b).

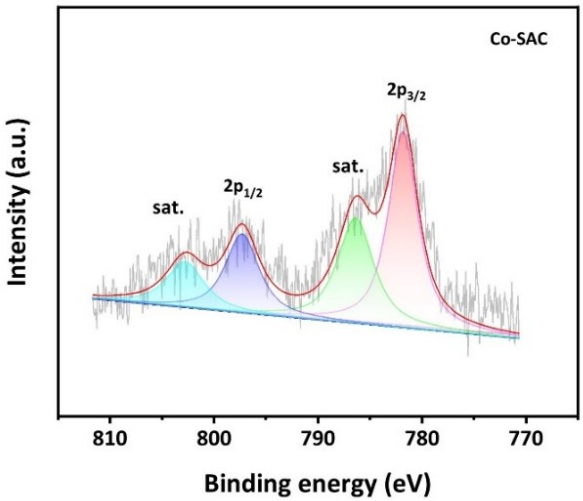

Figure S27 The XPS patterns of Co-SAC catalysts after 130 h reaction.

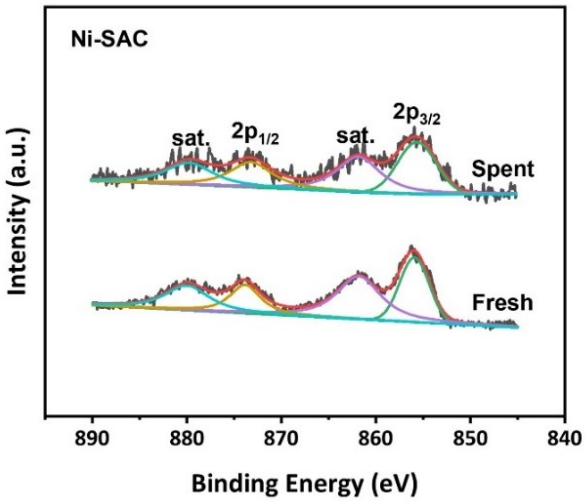

Figure S28 The XPS patterns of Ni-SAC catalysts after reaction

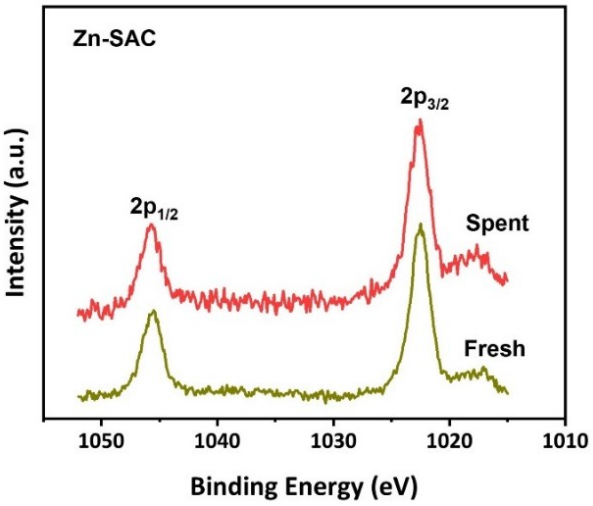

Figure S29 The XPS patterns of Zn-SAC catalysts after reaction.

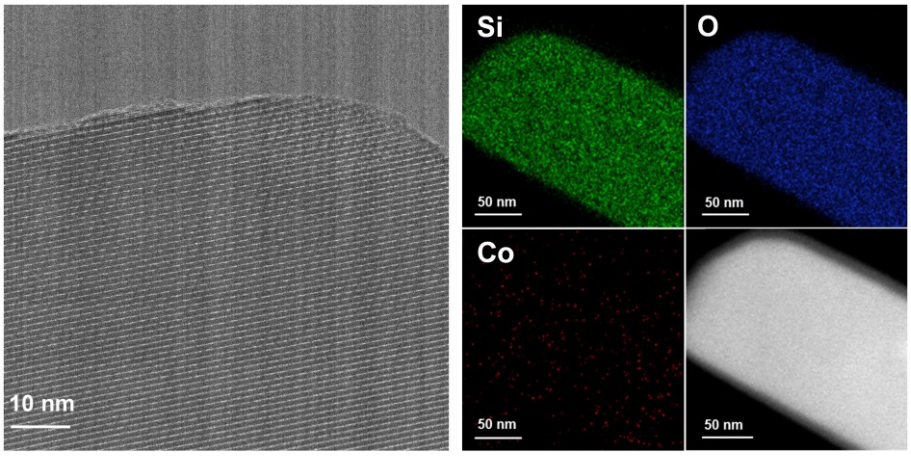

Figure S30 HADDF-STEM image, and the corresponding EDS mapping images of the fresh Co-SAC after 10 h reaction.

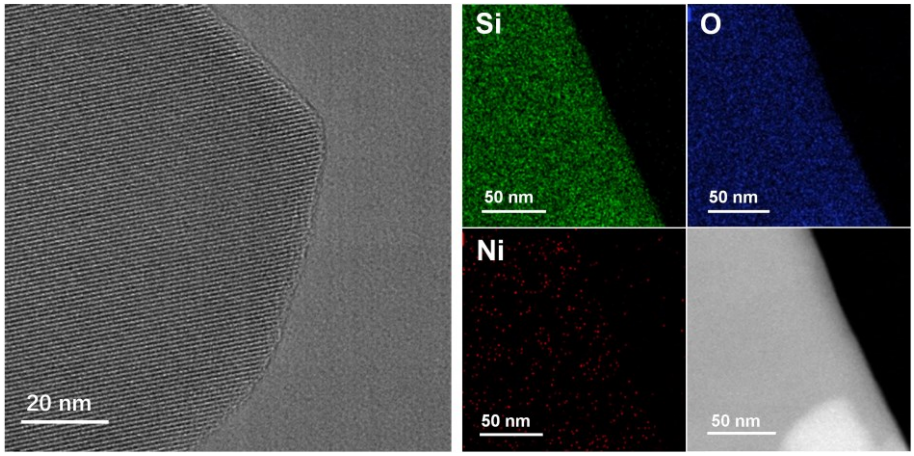

Figure S31 HADDF-STEM image and the corresponding EDS mapping images of the fresh Ni-SAC after 10 h reaction.

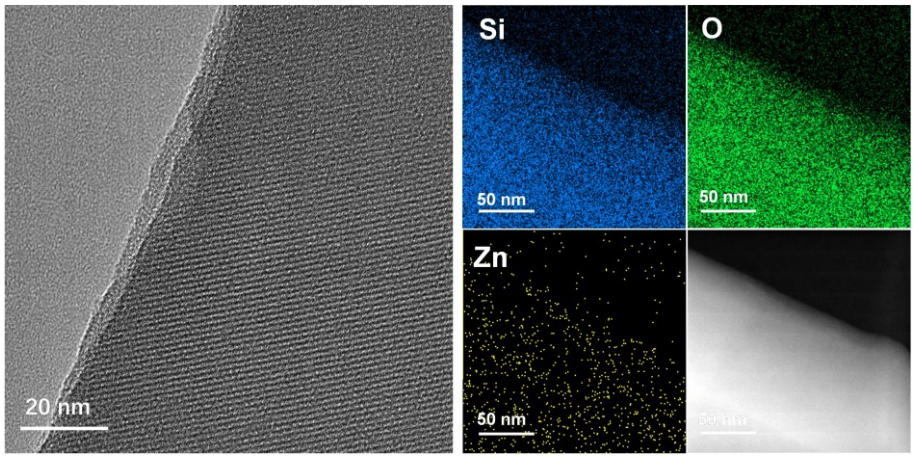

Figure S32 HADDF-STEM image and the corresponding EDS mapping images of the fresh Zn-SAC after 10h reaction.

Table S1. Structural parameters of M-SACs extracted from the EXAFS fitting ($S0^2$=0.85)

Sample	Path	C.N.	R (Å)	σ^2 (10^{-3}Å^2)	ΔE_0 (eV)	R-factor
Co-SAC	Co-O	3.2 ±0.5	1.96 ±0.012	2.75 ±1.75	-1.27 ±1.90	0.020
Ni-SAC	Ni-O	3.5 ±0.6	2.06 ±0.013	9.0*	-7.88 ±1.57	0.008
Zn-SAC	Zn-O	3.2 ±0.5	1.93 ±0.01	7.0 ±1.56	-0.11 ±1.47	0.014
Cu-SAC	Cu-O	3.3 ±0.3	1.94 ±0.007	4.6 ±1.01	-6.42 ±1.35	0.008

$S0^2$ is the amplitude reduction factor $S0^2$=0.85; CN is the coordination number; R is interatomic distance (the bond length between central atoms and surrounding coordination atoms); σ^2 is the Debye-Waller factor (a measure of thermal and static disorder in absorber-scatterer distances); ΔE_0 is edge-energy shift (the difference between the zero kinetic energy value of the sample and that of the theoretical model). R factor is used to value the goodness of the fitting. The obtained XAFS data was processed in Athena (version 0.9.26) for background, pre-edge line and post-edge line calibrations. Then Fourier transformed fitting was carried out in Artemis (version 0.9.26). The k^3 weighting, k-range of 3-12 Å^{-1} and R range of 1~3 Å were used for the fitting of foil; k-range of 2-11 Å^{-1} and R range of 1~3 Å were used for the fitting of samples.

Table S2. Comparison of the activity of catalysts in present work and reported literatures.

Catalyst	Temp. (°C)	Feed composition	Con. (%)	Sel. (%)	K_d (h^{-1})	Ref.
K-PtSn@MFI	600	C_3H_8: He= 6: 19	38.7	97	0.012	1
K-PtSn@MFI	600	C_3H_8: He= 5: 16	71	88	0.019	2
Pt/Fe-3	550	C_3H_8: N_2 = 1: 3	47.5	90.5	0.012	3
PtSn/SiO_2	580	Pure C_3H_8	40.4	99	0.008	4
ZnO-S-1	550	C_3H_8: N_2 = 2: 3	30	90	0.49	5
ZnOx/S-1	600	C_3H_8: N_2 = 2: 3	30.8	88	0.008	6
Cu−ZnO@S-1	600	C_3H_8: H_2 = 7: 3	34.4	86.5	0.025	7
Co-MFI	580	C_3H_8: Ar= 1: 19	~58	97	-	8
Co-SBA-15	600	C_3H_8: H_2 = 1: 6	37	96	-	9
Co SAs/SiO_2	550	C_3H_8: N_2 =2:6.4	25	95.1	0.009	10
Co-acac@S-1	600	C_3H_8: N_2= 1: 19	47	94.7	0.028	11
Co-SAC	560	C_3H_8: N_2= 1: 4	40.3	98	0.0045	**This**

Table S3. Metal content and dispersion of M-SACs.

Catalyst	Metal content (wt%)		dispersion (%)
	fresh	spent	
Co-SAC	1.5	1.49	95.2
Ni-SAC	1.32	1.31	93.8
Cu-SAC	1.29	-	93.0
Zn-SAC	1.17	1.15	92.5

References:

1. Liu, L. C. et al. Structural modulation and direct measurement of subnanometric bimetallic PtSn clusters confined in zeolites. *Nat. Catal.* **2020**, *3*, 628-638.

2. Liu, L. C. et al. Regioselective generation and reactivity control of subnanometric platinum clusters in eolites for high-temperature catalysis. *Nat. Mater.* **2019**, *18,* 866-873.

3. Liu, H. et al. Isolated Pt Species Anchored by Hierarchical-like Heteroatomic Fe- Silicalite-1 Catalyze Propane Dehydrogenation near the Thermodynamic Limit. *ACS Catal.* **2023,** *13,* 2928-2936.

4. Motagamwala, A. H., Almallahi, R., Wortman, J., Igenegbai, V. O. & Linic, S. Stable and selective catalysts for propane dehydrogenation operating at thermodynamic limit. *Science* **2021**, *373,* 217-222.

5. Zhao, D. et al. In situ formation of ZnOx species for efficient propane dehydrogenation. *Nature* **2021,** *599,* 234-238.

6. Zhao, D. et al. Controlling Reaction-Induced Loss of Active Sites in ZnOx/Silicalite-1for Durable Nonoxidative Propane Dehydrogenation. *ACS Catal.* **2022,***12*, 4608-4617

7. Song, S. J. et al. Silicalite-1 Stabilizes Zn-Hydride Species for Efficient Propane Dehydrogenation. *ACS Catal*. **2022,** *12,* 5997-6006.

8. Hu, Z. P. et al. Atomic Insight into the Local Structure and Microenvironment of Isolated Co Motifs in MFI Zeolite Frameworks for Propane Dehydrogenation. *J. Am. Chem. Soc.* **2022,** 144, 12127-12137

9. Huang, Z. J. et al. Illustrating a new understanding of adsorbed water on silica for inducing tetrahedral cobalt(II) for propane dehydrogenation. *Nat. Commun.* **2023,** *14,* 100.

10. Wang, W. Y. et al. Single Co Sites in Ordered SiO_2 Channels for Boosting Nonoxidative Propane Dehydrogenation. *ACS Catal.* **2022,** *12,* 2632-2638.

11. Song, S. J. et al. In situ encapsulated subnanometric CoO clusters within silicalite-1 zeolite for efficient propane dehydrogenation. *AIChE J.***2022** ,*68*, e17451.